Parallel-core-type polarization rotator for silicon wire waveguide platform

Hiroshi Fukuda[1,2,*] and Kazumi Wada[1]

[1]*The University of Tokyo, School of Material Engineering, 7-3-1 Hongo, Chiyoda, Tokyo, Japan*
[2]*NTT, Microsystem Integration Laboratories, Morinosato-Wakamiya, Atsugi, Kanagawa, Japan*
**Corresponding author: fukuda@microphotonics.t.u-tokyo.ac.jp*

Received February 5, 2014; revised March 14, 2014; accepted March 17, 2014;
posted March 18, 2014 (Doc. ID 205977); published April 11, 2014

We describe a polarization rotator based on a parallel-core structure consisting of a silicon nanowire waveguide and a silicon-nitride waveguide. The 60-μm-long rotator provides a polarization extinction ratio of more than 10 dB with excess loss of less than 1 dB. In addition, the extremely wide bandwidth of more than 150 nm expected from calculations is confirmed in experiments. A study of the fabrication tolerance of our rotator indicates that fabrication error of around 25 nm is allowable. © 2014 Chinese Laser Press

OCIS codes: (130.5440) Polarization-selective devices; (230.5440) Polarization-selective devices.
http://dx.doi.org/10.1364/PRJ.2.000A14

1. INTRODUCTION

Silicon (Si) microphotonics is an attractive candidate for next-generation photonic platforms [1]. Telecommunications applications require wideband devices in order to transport large amounts of information. For Si microphotonic devices, a multichannel configuration provides the potential for meeting the demands of high-speed data transmission. Thanks to the high refractive index contrast between Si core and silica cladding, Si microphotonic devices can be fabricated with very small footprints, and numerous devices, including modulators and detectors, can be integrated with high density [2–5]. Therefore, the total data rate would become large for Si microphotonic integrated circuits. However, there are some additional requirements for near-future telecommunications applications.

With dense wavelength division multiplexing, there will be a limitation on the channel number. Numerous multiplexed lightwaves would increase the power density in an optical fiber, generate cross interaction among channels because of nonlinear optical effects in the fiber core, and result in signal deterioration. Thus, the next generation of optical networks will require a multilevel modulation coding system. Dual polarization quadrature phase shift keying (DP-QPSK) is a promising technique for future wideband telecommunications architectures. The capability to handle DP-QPSK signals depends on polarization manipulation, including polarization separation and rotation. Therefore, polarization manipulation will become one of the most important techniques in future Si microphotonics.

Meanwhile long-distance telecommunications has several technical issues, which are not of concern in short-reach communications. One is polarization dependence. Since telecom equipment can be exposed to underground, undersea, and other severe environments, where there are large temperature variations and large mechanical vibrations, all devices must be polarization independent. Si photonic wire waveguides produce large structural birefringence, which degrades the quality of transmission data, and the birefringence is so large that external electronic or photonic circuits cannot compensate for it. Therefore, polarization manipulation techniques are again indispensable.

2. TECHNICAL ISSUES FOR POLARIZATION MANIPULATION

Several kinds of devices for polarization manipulation in Si microphotonics have been proposed and demonstrated [6–16]. A two-dimensional grating coupler, which couples orthogonal modes from a fiber into identical modes of two waveguides, has been developed [6,7]. This device efficiently achieves polarization splitting with a small footprint, and couples both fiber polarizations to the transverse electric (TE) mode of their own photonic wire waveguide. Therefore, no additional on-chip TE to transverse magnetic (TM), or TM to TE polarization conversion is needed. The efficient bandwidth, however, is quite narrow because the grating has inherently strong wavelength dependences.

Another approach is polarization diversity. This architecture employs polarization splitters and rotators. The polarization splitter can be realized by using the large birefringence of the Si waveguide, i.e., a simple directional coupler consisting of two oblong cores. However, the challenging issue is to fabricate the rotators, so researchers have investigated various types. A mode-evolution-based [8,9] rotator in a Si photonic wire waveguide achieved a polarization extinction ratio (PER) of around 15 dB. However, since the mode evolution requires long propagation distance of light, the device becomes large. Higher-mode hybridization [10,11] and asymmetrical directional coupler [12,13] techniques are also powerful for polarization manipulation, especially for rotation and conversion. Their characteristics are easily affected by the dimensions of their structures. Plasmon-based waveguides [14,15] can realize novel polarization controls, but have unavoidable losses.

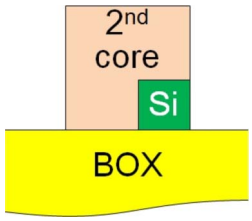

Fig. 1. Cross-sectional view of double-core rotator.

Since a double-core polarization rotator [16], which is based on the mode-coupling technique, has an optimum propagation distance shorter than that of the mode-evolution type, and marginally large fabrication tolerance, it can take full advantage of Si microphotonics. However, such rotators had two serious drawbacks regarding insertion loss and bandwidth. A cross-sectional view of a double-core rotator is shown in Fig. 1. A Si waveguide with a square core is embedded in a second waveguide whose core is larger than the Si waveguide's. The waveguides have offsets both horizontally and vertically, and the left- and down-side edges of the Si waveguide close up the corresponding edges of the second waveguide. The eigenaxes of such an off-axis double-core structure are tilted toward the substrate. The difference in effective indices between the two orthogonal eigenmodes produces polarization rotation when the polarization of an incident light is parallel (TE) or orthogonal (TM) to the substrate. Figure 2 shows measured transmission spectra of a double-core rotator. The polarization of the input light was set to TM. The difference in the graphs between Figs. 2(a) and 2(b) is how they were normalized. The spectra in Fig. 2(a) are normalized by the transmittance of a simple Si waveguide, which was fabricated on the same chip as the rotator, and whose length is almost the same as that of a waveguide with the rotator. The reference spectrum is the transmittance of a fiber in Fig. 2(b). A larger transmittance of TE than that of TM indicates that the rotator works well. However, in Fig. 2(b), one can see a sharp spectral dip around the operation wavelength of 1500 nm for both TE and TM. This spectral dip is caused by optical absorption by amino bonds (-NH-). The second core of the double-core rotator is made of silicon oxinitride (SiO_xN_y), which contains -NH- bonds. These bonds have huge optical absorption around the wavelength of 1500 nm. In addition, the SiO_xN_y film is deposited on the whole wafer, and it cannot be removed selectively because the etching ratio of SiO_xN_y is close to that of Si. Therefore SiO_xN_y covers not only the rotator but also the other waveguides, which results in large optical absorption.

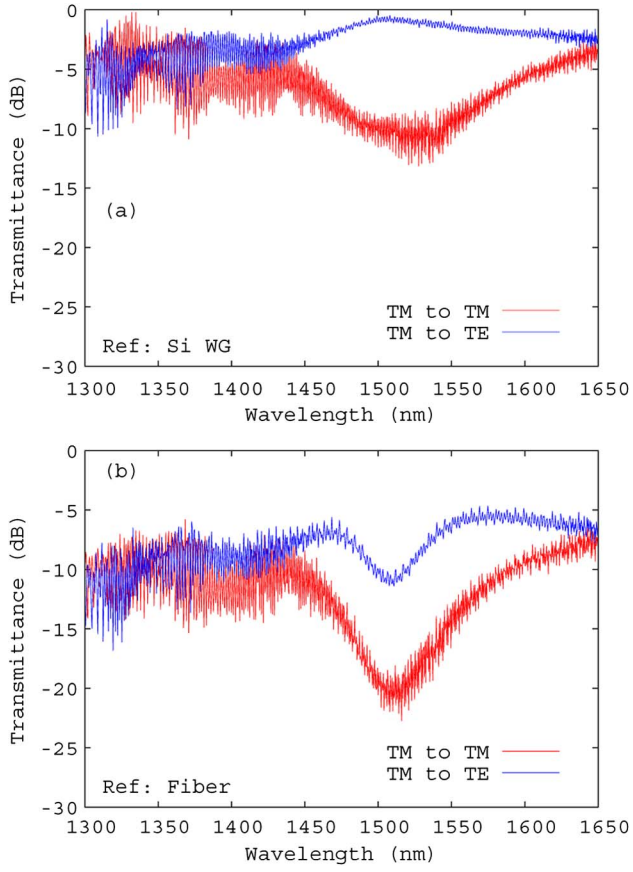

Fig. 2. Transmission spectra of double-core rotator. (a) Normalized by transmission of normal Si wire waveguide. (b) Normalized by transmission of a fiber.

Furthermore, there are pros and cons of a large refractive index of the second core. Figure 3 shows the estimated PERs of double-core rotators with various refractive indices of the second core. A large index indicates wide bandwidth. This large refractive index layer is utilized not only as a second core but also as an overcladding for other waveguides. The communication protocol has required –10 dB PER, which indicates the operation wavelength of the double-core rotator ranges from 1500 to 1600 nm when $n = 1.6$. The prediction is reproduced in Fig. 2. A waveguide with such high-index overcladding cannot be bent sharply. Calculated bending losses of Si waveguides with various refractive indices of overcladding (n_{oc}) are shown in Fig. 4. The polarization of the light was TE at 1550 nm, the bending radius was set to 5 μm, and the Si core was 400 nm wide and 200 nm high. Calculated electrical fields are shown in insets. The mode profile of the bending waveguide with large index overcladding is apparently distorted. The bending loss is negligible for n_{oc} of less than 1.8 but suddenly becomes large around n_{oc} of more than 1.9. When n_{oc} is 2.2, the bending loss reaches 0.2 dB for a 90 deg corner. If an optical circuit contains 10 corners, the total bending loss becomes 2 dB. Since this value is not acceptable for practical devices, the radius of bending has

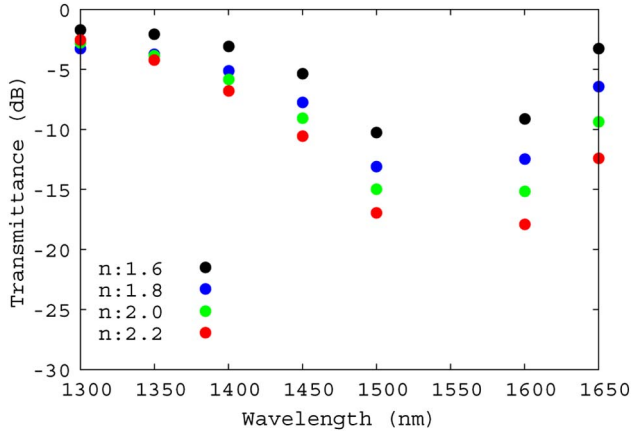

Fig. 3. Calculated transmission spectra of the double-core rotator with various refractive indices of overcladding.

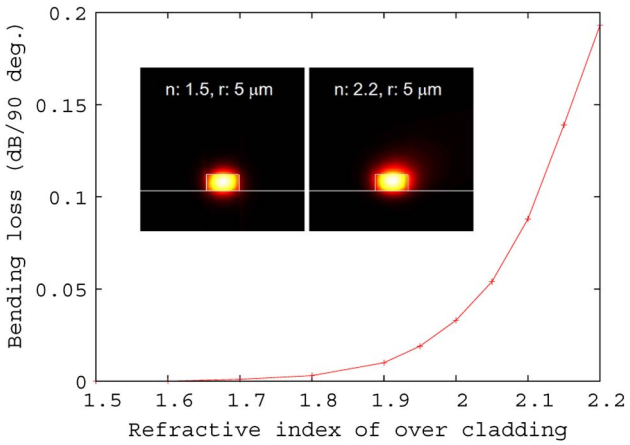

Fig. 4. Calculated bending loss of the Si waveguide with 400 nm × 200 nm core for the bending radius of 5 μm as a function of the refractive index of overcladding.

to be extended to reduce the bending loss. Therefore, it is difficult to realize a photonic circuit with a wideband rotator in a small footprint.

3. PARALLEL-CORE POLARIZATION ROTATOR

To overcome these problems, we propose a new structure for the polarization rotator: parallel-core type. Called the parallel-core rotator, its basic concept is almost the same as that of the double-core type. Like the double-core rotator, it also equips the Si core and second core, but the second core does not cover the Si core as shown in Fig. 5. Both of the cores are embedded in SiO_2 overcladding. This configuration of separation enables us to remove the high-index film except for that near the second core of the rotator. Therefore, the parallel core does not have the problem of optical absorption. Polarization rotation angle, θ, is described by

$$\theta = \frac{\pi L \Delta n}{\lambda}, \tag{1}$$

where L is the propagation length, Δn is the difference in the effective indices between the two orthogonal eigenmodes, and λ is the operation wavelength. The rotator length to accomplish 90 deg rotation, $L_{\pi/2}$, is described by

$$L_{\pi/2} = \frac{\lambda}{2\Delta n}. \tag{2}$$

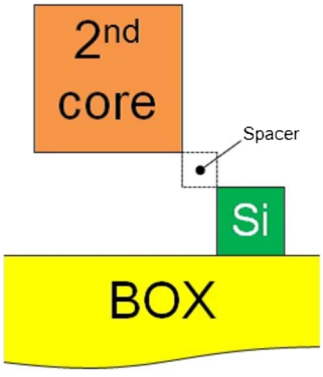

Fig. 5. Cross-sectional view of the parallel-core rotator.

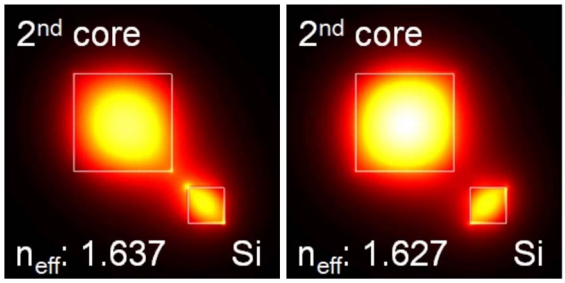

Fig. 6. Eigenmodes of the parallel-core structure.

The efficient wavelength range thus becomes wider for a device with shorter propagation length. Design parameters for the parallel-core rotator are the Si core size, second-core size, second-core index, and spacer size. Spacer means the gap between two cores as shown in Fig. 5. The spacer increases a degree of freedom of design, and enables wideband characteristics if the size of the spacer can be optimized. The spacer controls the coupling efficiency between two cores, and the effective indices of the coupled waveguide. These parameters are functions of operating wavelength. Therefore, the optimization of the spacer size can improve the wavelength dependence of the rotator, resulting in wideband characteristics.

First, the Si core size was determined to be 220 nm square because a normal silicon-on-insulator (SOI) wafer has a 220-nm-thick SOI layer. A smaller spacer is better because the coupling of the two cores becomes large, but it is difficult to create a thin film with a smooth and flat surface because the surface under the second core would be planarized by a chemical–mechanical polishing technique. We therefore chose a spacer film thickness of 100 nm to maintain an accurate thickness of spacer film and small interface roughness. Next we defined the parameters for the second core. The second core's index was set to 2.0 because this value is close to the refractive index of silicon nitride (Si_3N_4). Its size was set to 600 nm square, which satisfies the single-mode condition. The mode profiles of the two orthogonal eigenmodes for the rotator with the parameters defined above are shown in Fig. 6. Since the effective indices of these modes are 1.637 and 1.627, respectively, the required rotator length would be 78 μm.

A schematic top view of a fabricated rotator is shown in Fig. 7. The Si wires for the input and output are 220 nm high and 500 nm wide. Their cores are adiabatically connected to the 220 nm square Si core by Si taper waveguides. Although the second core and small Si core satisfy the single-mode condition, there are high-order modes in a coupled waveguide. To reduce the higher-order mode loss, we introduced adiabatic taper couplers at the input and output of the rotator. The rotator length was set to 60 μm, which is shorter than the

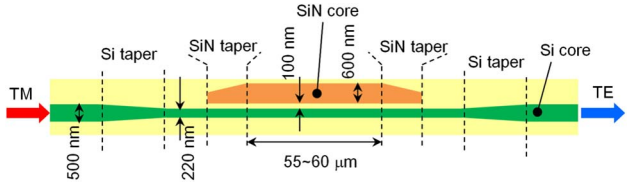

Fig. 7. Schematic top view of the parallel-core rotator.

value estimated from the calculated effective indices because the taper coupler would also work as a rotator.

4. EXPERIMENT

A. Polarization Rotation Characteristics

A light source was a superluminescent diode (SLD) that covered the wavelength range from 1300 to 1650 nm. Light from the SLD was filtered through a polarizer, and linear polarized light was coupled into a polarization maintaining fiber. At the coupling between the fiber and Si waveguide, the angle of polarization of incident light was measured with a near-infrared camera through a rotatable Glan–Thompson prism and set to the TM mode by rotating the fiber. Output light was again filtered through a polarizer and measured with an optical spectrum analyzer.

Transmission spectra for the parallel-core rotator are shown in Fig. 8. Red and blue lines represent the transmittances of TM and TE components, respectively. Solid and broken lines in Fig. 8(a) correspond to measured and calculated transmittances. The calculation was carried out by the eigenmode expansion method. The difference in the graphs between Figs. 8(a) and 8(b) is how they were normalized. The spectra in Fig. 8(a) are normalized by the transmittance of a simple Si waveguide, which was fabricated on the same chip as the rotator and whose length is almost the same as a waveguide with the rotator. The reference spectrum is the transmittance of a fiber in Fig. 8(b). The larger transmittance of TE than that of TM indicates that the rotator works well. The PER was about 10 dB, and the excess loss was less than 1 dB. In addition, in Fig. 8(b), there is no spectral dip around the operation wavelength of 1500 nm for both TE and TM. This means that the parallel-core structure can successfully reduce the effect of optical absorption caused by -NH- bonds. Furthermore, the parallel-core rotator has larger bandwidth than the double-core type. The 10 dB bandwidth covers the wavelength range from S to L bands (1460–1625 nm). Measured results agreed with calculated ones. Thus we can conclude that the parallel-core type would be advantageous over the double-core type.

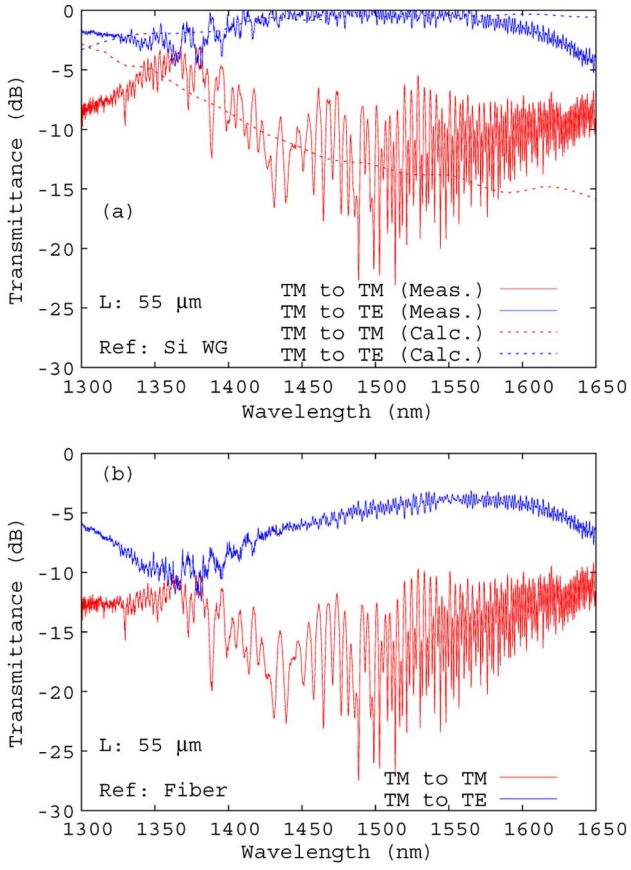

Fig. 8. Transmission spectra of the parallel-core rotator. (a) Normalized by transmission of normal Si wire waveguide. (b) Normalized by transmission of a fiber.

The unlevel structure in the spectra of the stop light (TM component) is caused by slight misalightment of the rotation angle of the input fiber. In this experiment, the length between the Si waveguide and the start of the rotator is about 1.6 mm. This section is the normal Si wire with a 500 nm × 220 nm core. Thus, if the polarization plane of incident light is tilted toward the substrate, ripples appear in the transmission spectrum. The wavelength interval of ripples $\Delta\lambda$ can be calculated as

$$\Delta\lambda = \frac{\lambda^2}{(n_g^{\mathrm{TE}} - n_g^{\mathrm{TM}})L}, \tag{3}$$

where λ is the operating wavelength, n_g^{TE} is the group index of the TE mode, n_g^{TM} is the group index of the TM mode, and L is the waveguide length. For a Si wire with a 500 nm × 220 nm core, around the wavelength of 1550 nm, n_g^{TE} and n_g^{TM} are 4.06 and 3.66, respectively. Calculated $\Delta\lambda$ is 3.8 nm, which agrees with the value in Fig. 8.

B. Fabrication Tolerance

For a practical device, it is important to estimate fabrication tolerance. The spacer size is the most critical parameter for fabrication of the parallel-core rotator. Calculated transmittance is shown in Fig. 9 as a function of the spacer width. Since this device was optimized for a rotator with a 100 nm wide spacer, the PER reaches the maximum at the width of 100 nm. The estimation says that both narrow and wide spacers decrease the PERs and increase excess losses. The spacer width must be 10 ± 20 nm to maintain a PER of more than 10 dB.

Figure 10 shows measured results for the rotators with spacers of 50, 100, and 150 nm in width. A rotator with a

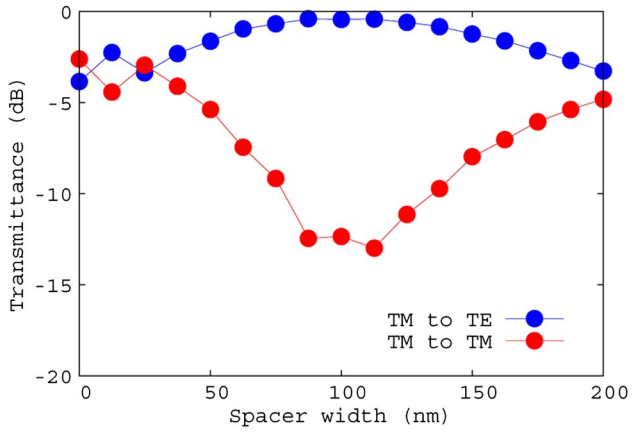

Fig. 9. Calculated transmittance of the parallel-core rotator with various spacer widths.

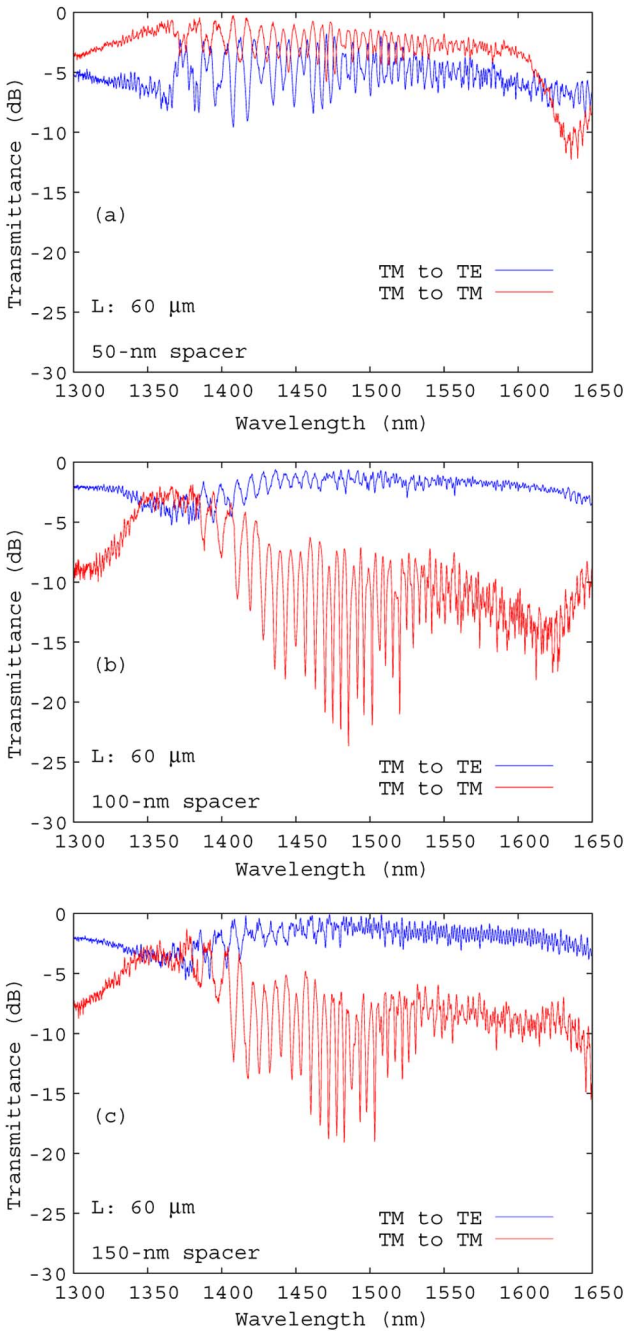

Fig. 10. Transmission spectra of the parallel-core rotator. (a) Spacer width, 50 nm. (b) Spacer width, 100 nm. (c) Spacer width, 150 nm.

50 nm spacer has poor performance as a rotator. Since the transmittance of TM is slightly larger than that of TE, the actual spacer width would be narrower than the designed value. The performance of rotators with a 100 nm spacer and 150 nm spacer is almost the same. If the actual spacer width were 25 nm narrower than the designed one, all experimental results would be explained by the calculation model of Fig. 9. Therefore, we can conclude that the fabrication tolerance of the parallel-core rotator is ±25 nm. This value is practical and acceptable for current fabrication technology.

5. CONCLUSION

We demonstrated a parallel-core polarization rotator consisting of a Si wire waveguide and a Si_3N_4 waveguide. A 60-μm-long rotator provides a PER of 10 dB with excess loss of less than 1 dB. Moreover the 10 dB bandwidth covers a wavelength range of more than 150 nm. The spacer between the Si core and the Si_3N_4 core resolves the crucial problem of optical absorption in the wavelength range of around 1500 nm. Our polarization rotator is suitable for mass production because it utilizes just planar fabrication, and allows fabrication error of around 25 nm. We believe that our polarization rotator represents a significant step toward accomplishing DP-QPSK devices and an integrated optical circuit with polarization diversity based on the Si wire waveguide platform.

REFERENCES

1. L. Vivian and L. Pavesi, *Handbook of Silicon Photonics* (Taylor & Francis, 2013).
2. Y. Urino, Y. Noguchi, M. Noguchi, M. Imai, M. Yamagishi, S. Saitou, N. Hirayama, M. Takahashi, H. Takahashi, E. Saito, M. Okano, T. Shimizu, N. Hatori, M. Ishizaka, T. Yamamoto, T. Baba, T. Akagawa, S. Akiyama, T. Usuki, D. Okamoto, M. Miura, J. Fujikata, D. Shimura, H. Okayama, H. Yaegashi, T. Tsuchizawa, K. Yamada, M. Mori, T. Horikawa, T. Nakamura, and Y. Arakawa, "Demonstration of 12.5-Gbps optical interconnects integrated with lasers, optical splitters, optical modulators and photodetectors on a single silicon substrate," Opt. Express **20**, B256–B263 (2012).
3. http://www.mellanox.com/.
4. http://www.luxtera.com/.
5. Z. Fang, Q. Y. Chen, and C. Z. Zhao, "A review of recent progress in lasers on silicon," Opt. Laser Technol. **46**, 103–110 (2013).
6. W. Bogaerts, D. Taillaert, P. Dumon, D. V. Thourhout, and R. Baets, "A polarization-diversity wavelength duplexer circuit in silicon-on-insulator photonic wires," Opt. Express **15**, 1567–1578 (2007).
7. F. V. Laere, W. Bogaerts, P. Dumon, G. Roalkens, D. V. Thourhout, and R. Baets, "Focusing polarization diversity grating couplers in silicon-on-insulator," J. Lightwave Technol. **27**, 612–618 (2009).
8. M. R. Watts, H. A. Haus, and E. P. Ippen, "Integrated mode-evolution-based polarization splitter," Opt. Lett. **30**, 967–969 (2005).
9. L. Chen, C. R. Doerr, and Y. Chen, "Compact polarization rotator on silicon for polarization-diversified circuits," Opt. Lett. **36**, 469–471 (2011).
10. D. Dai and J. E. Bowers, "Novel concept for ultracompact polarization splitter-rotator based on silicon nanowires," Opt. Express **19**, 10940–10949 (2011).
11. Y. Ding, H. Ou, and C. Peucheret, "Wideband polarization splitter and rotator with large fabrication tolerance and simple fabrication process," Opt. Lett. **38**, 1227–1229 (2013).
12. Y. Ding, L. Liu, C. Peucheret, and H. Ou, "Fabrication tolerant polarization splitter and rotator based on a tapered directional coupler," Opt. Express **20**, 20021–20027 (2012).
13. G. Chen, L. Chen, W. Ding, F. Sun, and R. Feng, "Ultra-short silicon-on-insulator (SOI) polarization rotator between a slot and a strip waveguide based on a nonlinear raised cosine flat-tip taper," Opt. Express **21**, 14888–14894 (2013).
14. J. Chee, S. Zhu, and G. Q. Lo, "CMOS compatible polarization splitter using hybrid plasmonic waveguide," Opt. Express **20**, 25345–25355 (2012).
15. M. H. El Sherif, O. S. Ahmed, M. H. Bakr, and M. A. Swillam, "Polarization-controlled excitation of multilevel plasmonic nano-circuits using single silicon nanowire," Opt. Express **20**, 12473–12486 (2012).
16. H. Fukuda, K. Yamada, T. Tsuchizawa, T. Watanabe, H. Shinojima, and S. Itabashi, "Polarization rotator based on silicon wire waveguides," Opt. Express **16**, 2628–2635 (2008).